

Article

# Integration of Drone and Satellite Imagery Improves Agricultural Management Agility

Michael Gbenga Ogungbuyi <sup>1</sup>, Caroline Mohammed <sup>1</sup>, Andrew M. Fischer <sup>2</sup>, Darren Turner <sup>3</sup>, Jason Whitehead <sup>4</sup> and Matthew Tom Harrison <sup>1,\*</sup>

<sup>1</sup> Tasmanian Institute of Agriculture, University of Tasmania, Launceston, TAS 7248, Australia; michael.ogungbuyi@utas.edu.au (M.G.O.); caroline.mohammed@utas.edu.au (C.M.)

<sup>2</sup> Institute for Marine and Antarctic Studies, University of Tasmania, Launceston, TAS 7248, Australia; andy.fischer@utas.edu.au

<sup>3</sup> School of Geography, Planning, and Spatial Sciences, College of Sciences and Engineering, University of Tasmania, Private Bag 78, Hobart, TAS 7001, Australia; darren.turner@utas.edu.au

<sup>4</sup> Cape Herbert Pty Ltd., Blackstone Heights, TAS 7250, Australia

\* Correspondence: matthew.harrison@utas.edu.au

**Abstract:** Effective agricultural management hinges upon timely decision-making. Here, we evaluated whether drone and satellite imagery could improve real-time and remote monitoring of pasture management. Using unmanned aerial systems (UAS), we quantified grassland biomass through changes in sward height pre- and post-grazing by sheep. As optical spectral data from Sentinel-2 satellite imagery is often hindered by cloud contamination, we assessed whether machine learning could help improve the accuracy of pasture biomass prognostics. The calibration of UAS biomass using field measurements from sward height change through 3D photogrammetry resulted in an improved regression ( $R^2 = 0.75$ , RMSE = 1240 kg DM/ha, and MAE = 980 kg DM/ha) compared with using the same field measurements with random forest-machine learning and Sentinel-2 imagery ( $R^2 = 0.56$ , RMSE = 2140 kg DM/ha, and MAE = 1585 kg DM/ha). The standard error of the mean (SEM) for the field biomass, derived from UAS-measured sward height changes, was 1240 kg DM/ha. When UAS data were integrated with the Sentinel-2-random forest model, SEM reduced from 1642 kg DM/ha to 1473 kg DM/ha, demonstrating that integration of UAS data improved model accuracy. We show that modelled biomass from 3D photogrammetry has significantly higher accuracy than that predicted from Sentinel-2 imagery with random forest modelling (S2-RF). Our study demonstrates that timely, accurate quantification of pasture biomass is conducive to improved decision-making agility, and that coupling of UAS with satellite imagery may improve the accuracy and timeliness of agricultural biomass prognostics.

**Keywords:** machine learning; artificial intelligence; drone; photogrammetry; pasture; grassland; monitoring; agricultural sustainability; adoption; practice change



**Citation:** Ogungbuyi, M.G.; Mohammed, C.; Fischer, A.M.; Turner, D.; Whitehead, J.; Harrison, M.T. Integration of Drone and Satellite Imagery Improves Agricultural Management Agility. *Remote Sens.* **2024**, *16*, 4688. <https://doi.org/10.3390/rs16244688>

Academic Editor: Michele Innangi

Received: 10 October 2024

Revised: 4 December 2024

Accepted: 13 December 2024

Published: 16 December 2024



**Copyright:** © 2024 by the authors. Licensee MDPI, Basel, Switzerland. This article is an open access article distributed under the terms and conditions of the Creative Commons Attribution (CC BY) license (<https://creativecommons.org/licenses/by/4.0/>).

## 1. Introduction

Grassland ecosystems play a significant role in supporting plant and animal diversity [1], providing ground cover to prevent erosion [2], and enabling agricultural production while contributing to global carbon sequestration [3,4]. Regular information pertaining to grassland structure is crucial to maintaining ecological health [5,6] and preventing overgrazing or natural adverse events [7] that threaten native biodiversity loss [8]. At the farm level, sustainable grazing management relies on timely monitoring of grassland components such as biomass quantity, ground cover, and residuals [9]. This helps control the carrying capacity index, which includes ecological, economic, environmental, and social factors [10]. By doing so, it is possible for livestock farmers and land managers to increase enterprise profitability while improving environmental stewardship [11]. However, traditional field-

measurement methods to monitor grazing activities are labour-intensive, and often lack spatially explicit information [2,12] that can be used to improve precision management.

Site-specific monitoring at the field scale (<1 ha) requires a high level of precision to provide real-time data and enable management decisions. This is particularly important in cell grazing systems, where high stocking density and regenerative practices are employed to improve grassland and soil productivity through trampling effects, regular movement of livestock, and programmed pasture-recovery periods [12,13]. Pre- and post-grazing monitoring provides information about biomass utilisation and indicates whether the reduction in grassland height has exceeded the target threshold to prevent overgrazing [14]. Unmanned aerial systems (UAS) equipped with a very high spatial resolution (1–5 mm) provide comprehensive grassland biomass and small-scale variation between and across fields [15]. However, the accuracy of UAS imagery is dictated by ground control points (GCP) necessary for integrating GPS georeferencing and processing large volumes of flight data on high-performance computing (HPC), which collectively can be cumbersome and capital-intensive [5,16,17]. Satellites offer wider coverage, although they have a lower spatial resolution, with timely imagery constrained by cloud interference [15]. Effective data fusion from multiple sensors has been used to gap-fill missing information due to cloud contamination and lower spatial resolution [2,18]. This is critical for enabling the provision of timely and accurate data to support intensive land use management, where rainfall and environmental factors play a key role in grassland productivity [3,4]. We hypothesise that integrating satellite data, such as Sentinel-2 [2], with unmanned aerial systems (UAS) may provide more timely imagery relating to biomass utilisation by livestock grazing [16].

Several studies have leveraged high-resolution satellite imagery, such as Planetscope, combined with predictive machine learning algorithms and UAS to detect biomass variability for grazing management at the field scale, typically around 1 ha [18,19], or over much larger areas [20,21]. However, the efficiency gains versus the cost, labour, and groundwork required with the use of such cloud-based technologies remains unclear.

Previous studies have used various point-cloud techniques, i.e., digital stereo aerial photographs or visible camera (5 cm) [5,16,17], multispectral cameras [16], Light Detection and Ranging (LiDAR) [22,23], and combination of visible camera and LiDAR [24–26] to model height of grassland swards using digital surface models (DSM). Normalised Difference Vegetation Index (NDVI) from a multispectral UAS camera with a random forest algorithm have been used to assess grassland biomass at the scale of one hectare [19]. These studies were based on woodland, arid, or semiarid ecosystems where the assessment of grassland focused on inter-canopy gaps [27] instead of vegetation density and canopy biomass typical of intensively managed grasslands [2]. Moreover, the methods presented did not account for biomass utilisation but rather estimated vegetation heights from shrubs, which are characteristic of arid rangeland systems [17]. Unlike LiDAR, 3D photogrammetry techniques are cost-effective and offer ortho-mosaicking capabilities (i.e., based on RGB) [24–26], making this data complementary and comparable to satellite spectral information. Although LiDAR is 3D-enabled, current spatial resolution in commercial markets typically ranges between 10–30 cm for most standard applications [28,29]. In contrast, UAS photogrammetry equipped with high-resolution cameras, such as the Zenmuse P1, offer sub-millimeter pixel ground resolution [30,31], suggesting that UAS photogrammetry may be more suited for capturing fine visual details and accurate prognostics of agricultural relevance, such as available biomass, green tissue, leaf litter, and nitrogen content.

In considering advances in timely assessment of the grassland ecosystems, Gillan et al. [17] argued that most studies that used remote sensing with UAS and satellites often compare co-registered spectral imagery with ground biomass sampling methods without multitemporal seasonality of images. Comparing satellite estimates, derived from machine learning models, with arguably the most accurate ground sampling method (i.e., destructively sampling) [32] using multitemporal spectral imagery is likely to provide more depth relating to the seasonality and temporal effects of land use dynamics, such as grassland utilisation, compared with traditional statistical analyses [2,33,34]. This is

because statistical analyses often overlook temporal effects when assessing the spectral variability of grazing activities [2,35]. Thus, the spectral changes in the vegetation canopy between pre- and post-grazing events across multiple small paddocks can be inferred from temporal and spectral analysis of Sentinel-2 imagery and othomosaic images using UAS photogrammetry modelling [2,34].

In the present study, historical management of the study site, Okehampton in south-eastern Tasmania, Australia, shows that the pastures have been exposed to poor agricultural practices including overgrazing during periods of low production (i.e., summer and drought), causing loss of native species and increasing ground exposure [35,36]. The dominance of sown species, together with historical land degradation of existing pasture species, including Phalaris (*Phalaris aquatic*) and Cocksfoot (*Dactylis glomerata*) [36] over perennial Ryegrass (*Lolium perenne*), Wallaby grass (*Austrodanthonia species*), and Kangaroo grass (*Themeda triandra*), underpinned our rationale to investigate avenues for improving sustainable grazing management.

Previous work suggests that pastures subject to adaptive grazing management can rejuvenate ecosystem services and build drought resilience through soil aggregation, porosity, and litter conversion, thus enhancing soil and pasture productivity through high stock density with frequent rotation [12,37,38]. Therefore, this study introduces multiple paddocks (or fields) to enable grassland monitoring through high stocking density and intensive grazing management. Site one consists of seasonal rotational grazing across 12 small paddocks. The other sites consisted of historically degraded grassland mainly dominated by Phalaris and Cocksfoot spear grass interspersed with native vegetation.

The aim of the study was to investigate whether remote sensing can enable accurate real-time grazing management. To achieve this, we addressed the following specific objectives:

Objective 1: To assess whether high-resolution UAS data could improve the accuracy and temporal resolution of biomass estimates derived from Sentinel-2 imagery, particularly in regions prone to frequent cloud cover. The goal was to calibrate UAS-derived sward height changes (pre- and post-grazing) from 3D photogrammetry model into field biomass and then use this to improve the Sentinel-2 random forest-enabled model, which is susceptible to cloud cover. Grassland biomass was sampled within 24 h of sheep grazing, with pre-grazing biomass cut data used for calibration. We regressed the change in height from UAS data (captured pre-grazing and post-grazing) against pre-grazing biomass cut data to convert height changes into biomass (kg DM/ha). This UAS-derived biomass data, captured at a 5 mm ground resolution, was then compared with biomass estimates from Sentinel-2 imagery, which utilised random forest-enabled spectral retrieval [33]. Sentinel-2, with its 5-day revisit cycle and 10 m spatial resolution, provided complementary monitoring data at the farm level.

Objective 2: Evaluate the effect of alternative sheep grazing regimes on the productivity and selective grazing of sown species (Phalaris and Cocksfoot). One paddock was used as a business-as-usual control, while another paddock included a mixture of sheep and pregnant ewes. We compared the sampled height data of Phalaris and Cocksfoot species in both paddocks with NDVI values derived from Sentinel-2 imagery to determine the impact of grazing intensity on pasture productivity.

Objective 1 is addressed through: (a) ground biomass sampling in the Vault and Bougainville paddocks (Site 1) and its relevance to UAS and Sentinel-2 imagery (Section 2.1.1); (b) UAS data collection and calibration (Section 2.3); and (c) Sentinel-2 data integration (Section 2.4). Objective 2 is discussed in Section 2.5, focusing on pasture botanical height measurement in the Cottage and Old Bougainville paddocks (Site 2) and comparisons with Sentinel-2-derived NDVI.

## 2. Material and Methods

### 2.1. Study Area and Field Data Collection

The study was conducted on a sheep enterprise near Triabunna, Tasmania, Australia (42°30'S, 147°59'E), with an annual rainfall of 648 mm and temperature ranges of 7 °C

(minimum) and 17 °C (maximum) [39]. The farm management aimed to maintain native and sown perennial vegetation communities by implementing more sustainable grazing practices [36].

Site 1 comprised “Vault” and “Bougainville” paddocks, each divided into six subplots of 0.25 ha (Figure 1). These subplots featured diverse native and sown ground cover species that were not degraded by agricultural management. The botanical composition included Cocksfoot, Phalaris, Ryegrass, Tall Fescue (*Festuca arundinacea*), Strawberry Clover (*Trifolium fragiferum*), Sub Clover (*Trifolium subterraneum*), Soft Brome (*Bromus hordeaceus*), Vulpia (*Vulpia bromoides*), Thistle (*Cirsium*), and Flatweed (*Hypocharis radicata*).

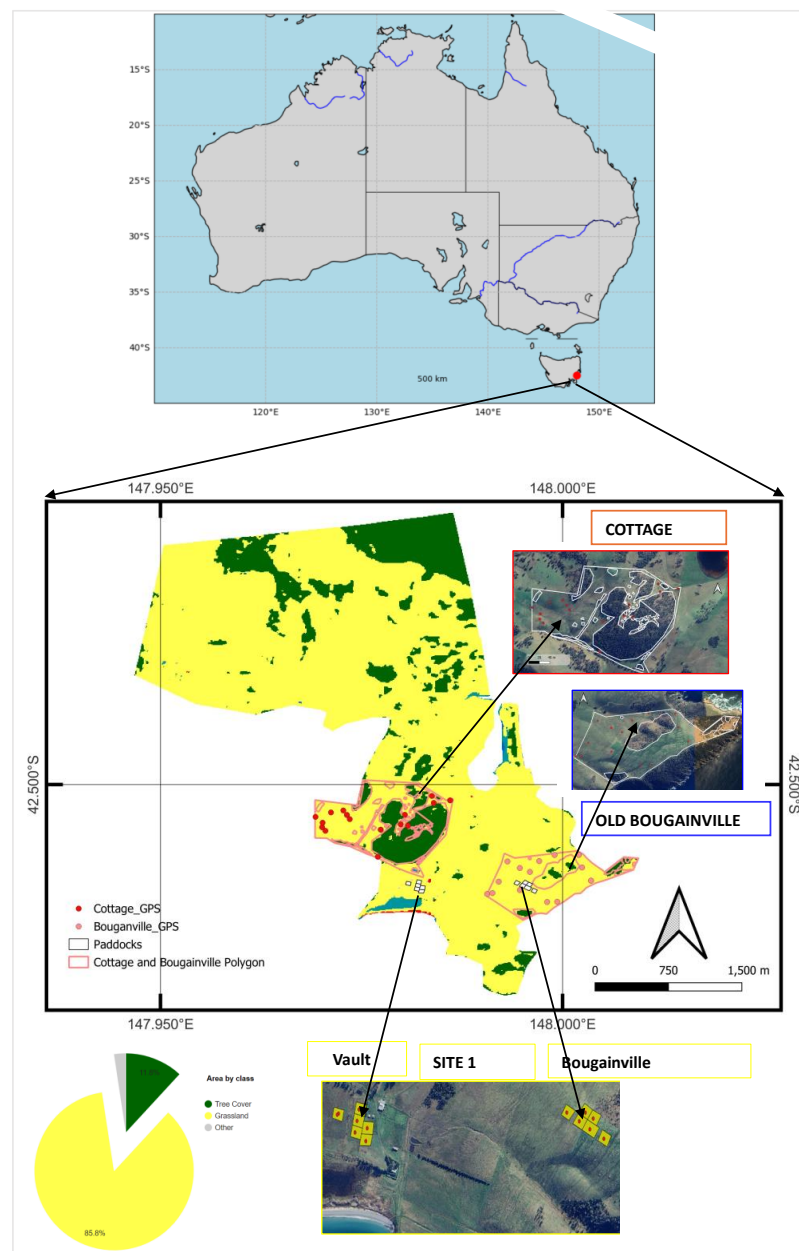


**Figure 1.** Location of commercial sheep farm “Okehampton” ( $42^{\circ}30'S$ ,  $147^{\circ}59'E$ ) near Triabunna, southeastern Tasmania, Australia. The yellow panel represents Site 1 (12 subplots of 0.25 ha), while the red panel represents Cottage paddock, and the blue panel represents Old Bougainville (located on the hilltop) is Site 2. Red dots depict sampling points located within each polygon of the imagery. The study site was mapped using 2020/21 global land cover from the European Space Agency (ESA), developed and validated with 10 m resolution of Sentinel-2 and Sentinel-1 imagery (<https://doi.org/10.5281/zenodo.5571936>).

Site 2 included the “Cottage Paddock” (118 ha) and the “Old Bougainville paddock” (80 ha) (Figure 1). During the experiment in spring 2019 (September to November), these paddocks were predominantly composed of sown species with Phalaris (*Phalaris aquatic*) and Cocksfoot (*Dactylis glomerata*) being dominant (Figure 2). They also contained fragmented native grasses, including Wallaby grass and Kangaroo grass. To restore native species, both the Cottage and Old Bougainville paddocks were treated with 2 L/ha of Glyphosate herbicide and 200 mL/ha of Ecopar herbicide to control weeds. All fields were rainfed.



**Figure 2.** Representative ground cover for the Cottage and Old Bougainville fields at Okehampton, Triabunna, Australia, January 2019. (a) Typical ground cover of Phalaris (*Phalaris aquatica* L.) shows a high proportion of bare ground and Flatweed (*Hypochaeris radicata*), (b) sheep track beside the heavily browsed ground from historical management. (c) Flatweed and Phalaris, and (d) healthy Phalaris, (e,f) were taken in November 2022 at the Vault paddock. Panel (e) shows an extremely high volume ( $>10,000$  kg DM/ha) of grassland, while (f) depicts a  $0.5 \times 0.5$  m quadrat, where physical biomass measurements were taken.

### 2.1.1. Vault and Bougainville Ground Sampling Protocol

The Vault and Bougainville paddocks underwent 1-day intensive grazing (7 a.m. to 7 p.m.) with a high stock density of 2000 DSE/ha (DSE = dry sheep equivalent) to improve pasture and soil productivity through trampling effects associated with regenerative grazing (see [12], Dry Sheep Equivalent is a standard unit used in Australia to compare the feed requirements of different classes, helping to assess the carrying capacity and productivity of grazing land). This high stocking density is assumed to flatten the biomass, stimulate soil microbial and aggregation, and reduce bare ground exposure [12,37,38]. The experiment was conducted from December 2021 to January 2023.

Standing biomass (above-ground biomass) was destructively sampled using five quadrats across each of the 12 paddocks, represented by the red dots in Site 1 as shown in Figure 1, between December 2021 and January 2023. Biomass harvest was performed using a battery-operated shearing handpiece at each  $0.5 \times 0.5$  m quadrat (Figure 2, panels (e) and (f)). The average of the five readings was computed as the standing biomass per paddock to minimise sampling error. For each sampling date, only pre-grazing ground sampling was conducted because one experienced operator was available. We scaled up this measurement to the paddock scale to conform to the 10 m resolution of Sentinel-2 imagery using Equation (1), since the satellite pixel is larger than the  $0.5 \times 0.5$  m quadrat. The  $0.5 \times 0.5$  m quadrat measurement was compared with 5 mm UAS (also known as drone) resolution.

$$\text{Total biomass}_{\text{paddock}} = \left( \frac{B_{\text{quadrat}}}{A_{\text{quadrat}}} \right) \times A_{\text{paddock}} \quad (1)$$

where:

$\text{Total biomass}_{\text{paddock}}$ : Total biomass in the paddock kg DM/ha.

$B_{\text{quadrat}}$ : Biomass in the sampling quadrat kg DM/ha.

$A_{\text{quadrat}}$ : Area of a single sampling quadrat kg DM/ha.

$A_{\text{paddock}}$ : Area of the entire paddock kg DM/ha.

For each destructive sampling, a non-destructive visual assessment of the estimated % species contribution to the standing biomass was made. Species assessment was based on ranking within the quadrat of each paddock [40]. The assumption was that the species composition would enhance pasture productivity due to the regenerative grazing management adopted [12].

### 2.1.2. Cottage and Old Bougainville Ground Sampling Protocol

These fields were stocked with 3–4-year-old Merino ewes. The Cottage paddock (Figure 1) was stocked at 700 DSE/ha and opened to adjoining paddocks to enable sheep to move freely across them. This business-as-usual treatment paddock served as the control. Old Bougainville (Figure 1) was stocked with a mixture of sheep and pregnant ewes at 350 DSE/ha and was closed off from adjoining paddocks, confining sheep to that paddock. Both paddocks were grazed for 5 days. The height of the dominant Phalaris and Cocksfoot species was randomly measured along the quadrats across both paddocks before and after grazing in October and November 2019. Sward height was measured (in cm) using a handheld ruler vertically from the ground surface to the highest point of the sward [17]. The location of each sampling point was recorded.

We observed whether the sheep preferred selective grazing of Phalaris or Cocksfoot species (Figure 2) in the two paddocks. Additionally, we examined the treatment effect of pregnant ewes during the lambing period, considering the increase in energetic requirements (DSE/ha) and subsequent increase on feed requirements [41,42]. Using the pasture height measurements, we correlated grazing intensity with Sentinel-2-derived NDVI.

To examine rainfall variability in the Cottage and Old Bougainville paddocks, gridded daily rainfall data at a 5 km resolution were obtained from the Australian Government of Bureau Meteorology as archived for November and December 2019 [43]. The daily rainfall

data was formatted into a weekly event to correlate with the grazing period (5 days) and referenced to pasture performance [12].

## 2.2. UAS Data and Processing for Vault and Bougainville at Site 1

Drone flights were undertaken by a DJI Matrice 300 remotely piloted aircraft system with a Zenmuse P1 camera, flying 40 m above ground level, yielding a ground resolution of 5 mm. The UAS is equipped with real-time-kinematics (RTK) for improved georectification. A GNSS survey of ground control point (GCP) tiles (Figure 3a) was completed on 4 January 2022, wherein paddock corners and sample plots (bricks and pins) were surveyed as recommended by James et al. [44]. Smaller tiles ( $0.1\text{ m} \times 0.1\text{ m}$ ) were installed to identify ground control points where drone measurements were taken. The survey campaign included Site 1 for Bougainville and Vault tiles and paddock corners. Trial flights were conducted over the plots to test the bricks and control points' visibility while refining data processing quality assurance. These plots were monitored with UAS from each successive flight, with 690 GNSS (RTK) survey points collected. Drone survey marks were sampled along diagonal transects within each grazing paddock (Figure 3c,d); in all cases, transects were positioned at least 10 m from paddock boundaries to avoid edge effects. The collected UAS images were processed to generate digital elevation models (DEM) and orthophotos. The workflow between the drone and field biomass measurement is provided in Figures 3 and 4.

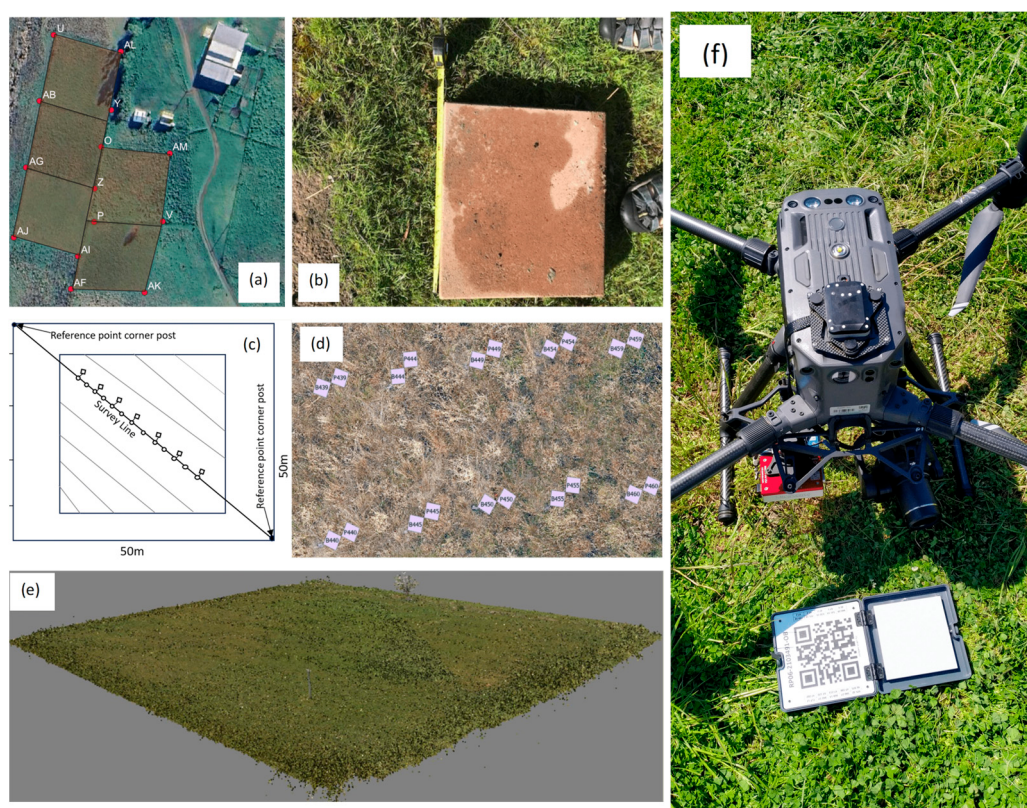


**Figure 3.** UAS campaign with survey protocol installations to compare UAS grass height measurements and destructively sampled biomass at the Okehampton farm, Triabunna, Tasmania, Australia. (a) Ground control point at the boundary of Vault paddocks, (b) bricks and pins installation to identify the ground control points, (c,d) diagonal transects along each paddock where sampled biomass data was collected, and (e) example of 3D point cloud photo of one of the processed UAS images captured for a pre-grazing event at Okehampton sheep grazing farm, Triabunna (photo taken in the pre-trial flight on 2 December 2021), and (f) DJI Matrice 300 RTK with Zenmuse P1. Images (b,d,e) were adopted from Harrison et al. [45].

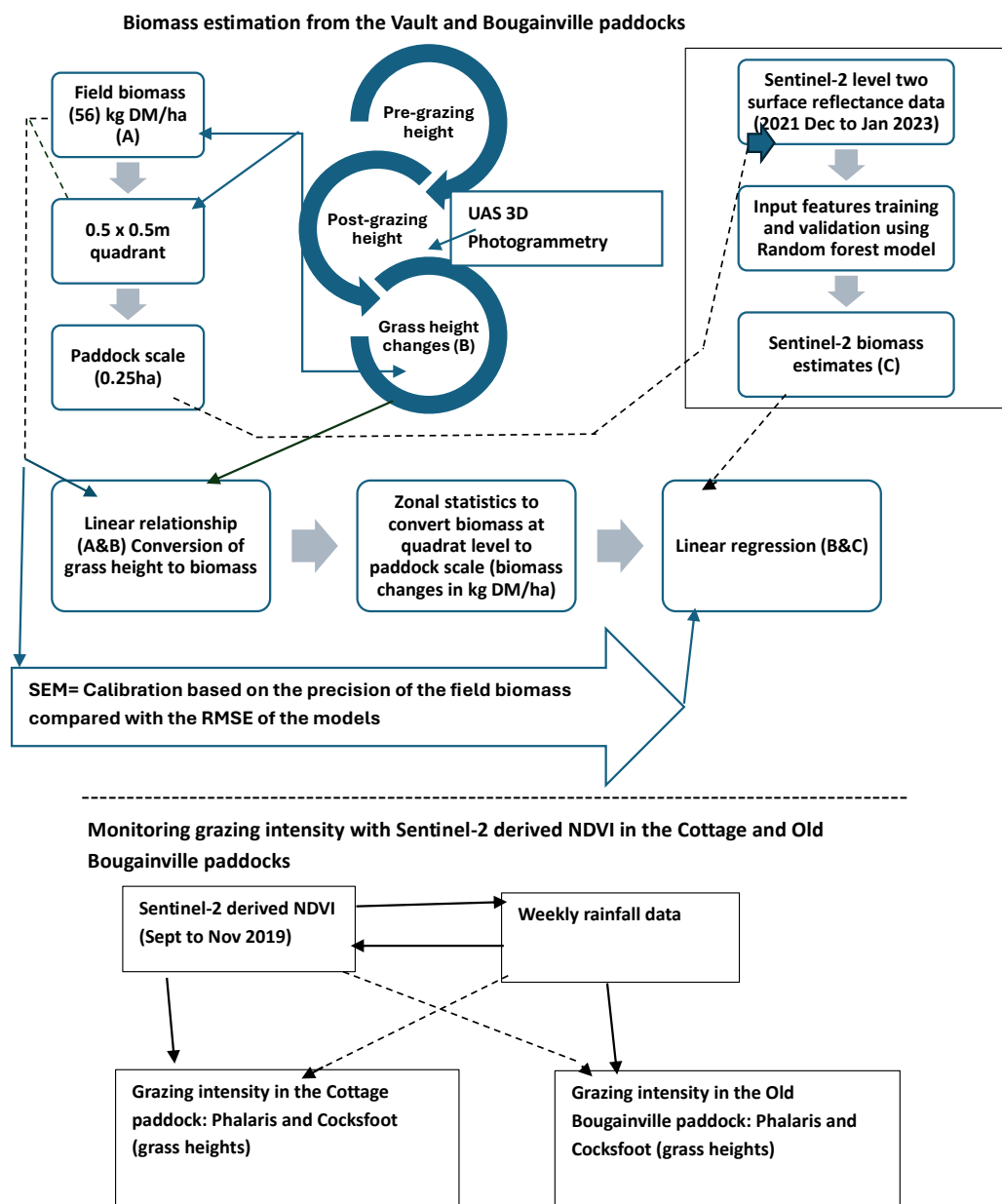


**Figure 4.** Workflow showing main components of the method.

### 2.3. Calibration of UAS Pasture Height Changes into Biomass for the Vault and Bougainville Paddocks at Site 1

Changes in sward height pre- and post-grazing events were monitored using a dedicated drone campaign. UAS pre-grazing measurements coincided with destructively sampled biomass. Ground quadrats were located using differential GPS (DGPS), allowing imagery to be overlaid and subsequent extraction of image metrics for comparison with ground surveys. Datasets were georeferenced using GCPs (tiles) at the corner of each trial paddock. UAS imagery was processed with high-performance computing (HPC) infrastructure, resulting in digital elevation models (DEMs) and orthophotos at 5 mm resolution. Using filtering by classes, all trees and artifacts were removed [46].

Pasture height differential pre- and post-grazing was calculated using flights before and after grazing (Figure 4). Pasture delta height was correlated with concurrent measurements of pasture biomass to determine the relationship between delta sward height and biomass. Following previous work [16], average pasture heights were estimated from

five quadrats along the same transects. Hence, the pasture height differential shown in the present paper comprise averages of five quadrats each of pre- and post-grazing flights.

Sward height changes derived from the 3D models were calibrated using pre-grazing biomass, which was destructively sampled from  $0.5 \times 0.5$  m quadrats (Section 2.1.1). We developed a linear relationship between these changes in sward height and the pre-grazing biomass data. The regression Equation (2) was determined by correlating the height changes with corresponding pre-grazing biomass measurements:

$$\text{Biomass} \left( \text{kg} \frac{\text{DM}}{\text{ha}} \right) = a \times \Delta \text{Height} + b \quad (2)$$

where  $\Delta \text{Height}$  is the delta sward height, and  $a$  and  $b$  are the slope and intercept of the regression. Equation (2) assumes that delta sward height is directly proportional to the change in biomass, allowing us to infer biomass change due to grazing. The linear relationship was used to create biomass maps for the Bougainville and Vault paddocks. To compare the drone biomass data with Sentinel-2 estimates, zonal statistics were performed to derive the mean biomass for each paddock (Figure 4). This ensured that the drone scale corresponded to the satellite scale. The calibrated UAS-derived biomass data were then used to improve the Sentinel-2 random forest-enabled model. Here, the UAS estimates, derived from the relationship between actual biomass and height changes, serve as a surrogate for actual biomass. This assumption was tested by comparing the standard error of the mean (SEM) of the actual biomass with the RMSE of the UAS data. The association between UAS and the sampled biomass was compared using the following regression statistics  $R^2$ , root mean square error (RMSE), and median absolute error (MAE).

#### 2.4. Sentinel-2 Data for Modelling Vault and Bougainville Biomass at Site 1 Using the Random Forest Algorithm

We downloaded 56 cloud-free Sentinel-2 level-images that have been corrected (i.e., level 2 surface reflectance) for atmospheric and topographic effects from Digital Earth Australia (<https://www.dea.ga.gov.au/products/dea-surface-reflectance>, accessed on 24 February 2023) for all dates that matched up (i.e., 5 December 2021 to 24 January 2023) with the sampled biomass data. The images underwent quality assurance, and cloudy pixels were removed using a cloud detection algorithm [47].

**Input Features:** We developed a random forest model from the 10 spectral bands as input features. We used 10 spectral bands from Sentinel-2 (b2, b3, b4, b5, b6, b7, b8, b8A, b11, and b12), which are particularly effective for terrestrial vegetation studies. These bands were selected because they are particularly useful for terrestrial applications, to allow the random forest model to capture a wide range of spectral information, which strengthens the machine learning process by training on the full spectrum of features [33,34].

**Dataset Partitioning:** Given the relatively small dataset of 56 samples, we partitioned the data into 75% training and 25% test sets and ensured that the training and test splits were randomised to avoid any potential bias. We set a random seed to ensure the reproducibility of the results.

#### Model Parameter and Optimisation:

- Number of Trees (n estimators): 50 trees were used to balance computational efficiency and performance.
- Maximum Tree Depth (maximum depth): We restricted tree depth to avoid overfitting, ensuring a good trade-off between complexity and accuracy.
- Feature Selection: The maximum number of features considered at each split followed the default setting (square root of the total number of input features) [33].
- Out-of-Bag (OOB) Error Estimation: OOB error estimates were used to assess training accuracy and minimise overfitting risks.

**Evaluation Metrics:** The model's performance was evaluated using  $R^2$ , RMSE, and MAE metrics, which provided insights into both overall model accuracy and error distribution. This allowed us to assess the model's ability to generalise to unseen data.

**Integration with UAS Data:** The Sentinel-2 random forest model outputs were compared with UAS-calibrated biomass data using linear regression. The test set performance was evaluated with the same metrics ( $R^2$ , RMSE, MAE), and a time series analysis was performed to examine the temporal dynamics of grassland productivity. This integration demonstrated how the high spatial resolution of UAS data complements the broader coverage of Sentinel-2 imagery.

## 2.5. Sentinel-2-Derived NDVI for Cottage and Old Bougainville at Site 2

The cottage and Old Bougainville paddocks were masked to remove trees and shrubs. We obtained cloud-free Sentinel-2 imagery from Digital Earth Australia [12] for Cottage and Old Bougainville paddocks. Images correspond to the dates of pasture-height measurements during the spring season (September to November 2019). We extracted the reflectance value per pixel based on visible bands 2 (blue), 3 (Green), 4 (Red), and 8 (NIR-1) bands. A cloud-detection algorithm was applied to remove all pixels affected by clouds [47]. NDVI for all GPS points representing Phalaris and Cocksfoot species height measurements was computed from red and NIR-1 bands. NDVI values were compared to the sampled heights of Phalaris and Cocksfoot using the correlation coefficient  $R^2$ .

## 3. Results

### 3.1. Biomass Calibration Using Delta Sward Height and Sentinel-2 with Random Forest Models

Figures 5–7 show that high-resolution drone data can be calibrated from the field biomass measurements, and at the same time be used to calibrate and validate Sentinel-2 models. The RMSE of the UAS model, at 1240 kg DM/ha, is slightly higher than the SEM of the sampled biomass, which is 1020 kg DM/ha, suggesting that the UAS model operates within the precision of the actual biomass. In general, both the UAS and Sentinel-2 random forest-enabled model (S2-RF) fall within the variability of the actual biomass, as indicated by the standard error bars in Figure 8.

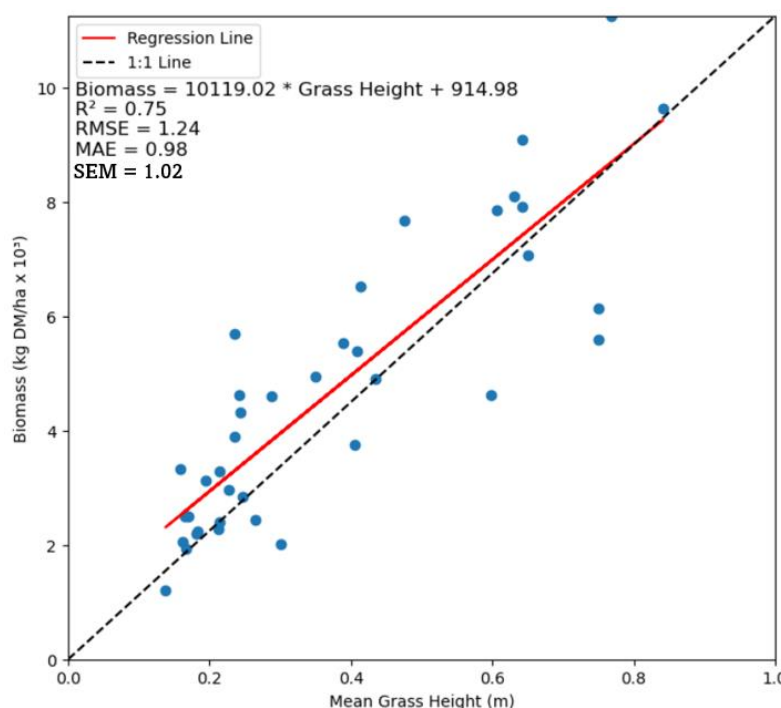


**Figure 5.** Relationship between mean sward height predicted from UAS and actual sampled biomass. The relationship translates delta pasture height (i.e., pasture height before and after grazing) into biomass.

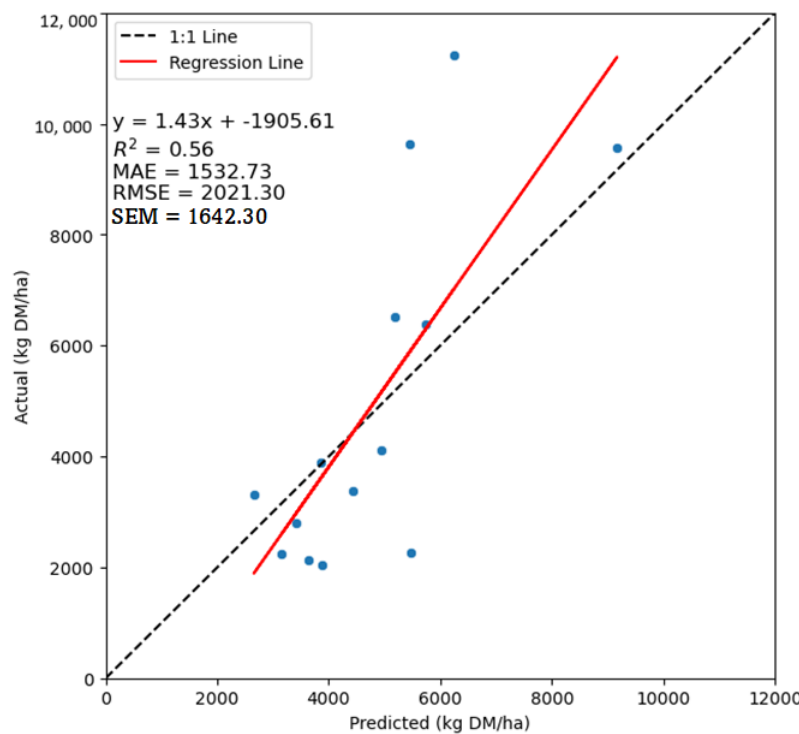


**Figure 6.** Sentinel–2 random forest model outputs compared with UAS–calibrated biomass data using linear regression for Vault and Bougainville.

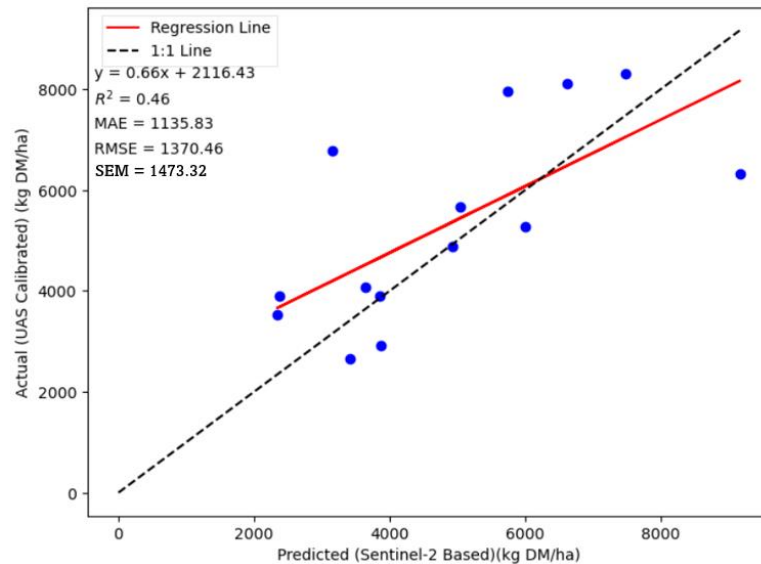


**Figure 7.** Sentinel-2 biomass calibration using UAS-derived biomass change data. Sentinel-2 data was based on the test set-obtained S2-RF-enabled model. Each point represents the average biomass at the paddock level for the drone and satellite. The calibration was conducted to elucidate whether UAS imagery could improve the temporal frequency and accuracy of biomass estimates from Sentinel-2 imagery, addressing challenges posed by frequent cloud cover obscuring satellite images in the high latitudes of southern Australia.

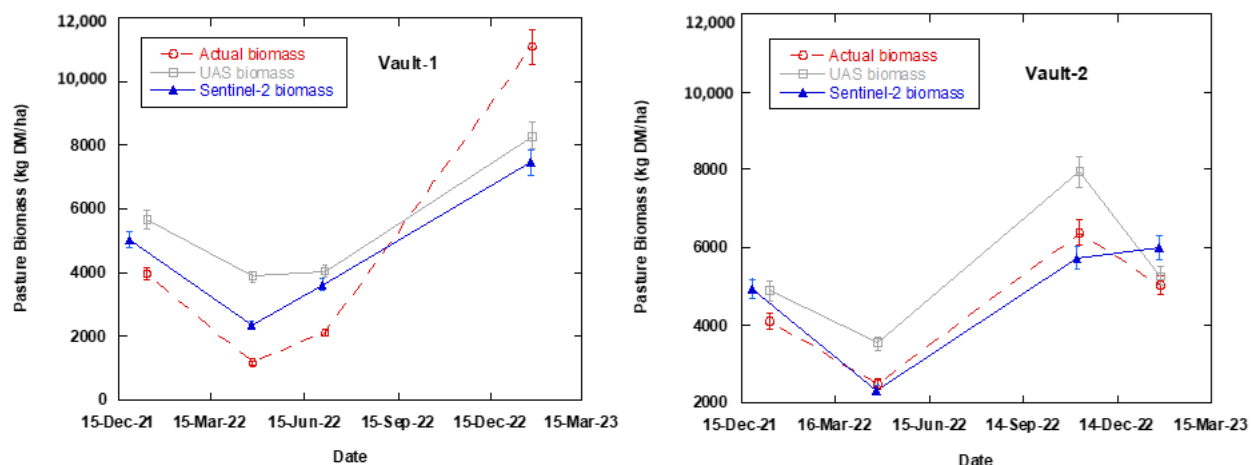


**Figure 8.** Comparison of the seasonality of UAS biomass in two representative paddocks against Sentinel-2 model estimates. The UAS model estimates biomass changes based on grass height variations between pre- and post-grazing events, while the Sentinel-2 estimates biomass using the nearest temporal imagery and a random forest algorithm. Each point represents the average biomass (mean) at the paddock level for both the drone and satellite.

The linear modelling of the change in grassland heights for pre- and post-grazing flights of UAS into biomass when calibrated with destructively sampled data yielded a strong relationship with a coefficient of determination ( $R^2$ ) of 0.75, RMSE = 1240 kg DM/ha, and MAE = 980 kg DM/ha (Figure 5). Equation (2) shows mean biomass computed for each of the 12 paddocks.

$$\text{Biomass} = 10,119 \times \text{Change in grass height} + 941$$

The large coefficient (10,119 kg DM/ha) indicates that small changes in grass height lead to significant changes in biomass. The high coefficient is partly attributed to very high sampled biomass (>10,000 kg DM/ha; Figures 4 and 5). The equation suggests that residual biomass post-grazing is around 914 kg DM/ha.

As shown in Figure 6, the evaluation of the random forest modelling using Sentinel-2 was reasonable ( $R^2 = 0.56$ , RMSE = 2140 kg DM/ha, and MAE = 1585 kg DM/ha). Comparing Figures 5 and 6, modelled biomass from 3D photogrammetry significantly outperformed the Sentinel-2 random forest-enabled model (S2-RF). The UAS demonstrated a stronger linear relationship with substantially lower error, highlighting its superiority over the S2-RF model.

Despite the lower  $R^2$  of 0.46 compared to the S2-RF  $R^2$  of 0.56, the UAS model exhibited lower error (RMSE = 1370 kg DM/ha and MAE = 1135 kg DM/ha). This indicates that while the S2-RF is better suited to explain the variance within treatments, the UAS model tends to produce more accurate estimates overall. This justifies the training of the field biomass dataset alongside spectral features using a random forest algorithm. These results suggest that the UAS-3D photogrammetry model is more accurate in predicting average subplot biomass, although the ability of such technology to reproduce subplot variability was lower than that of S2-RF.

Although Figures 5 and 6 show that both models tend to overestimate biomass, more than half of the calibrated data points from the UAS model show a higher overestimation of biomass relative to the S2-RF model. In contrast, about half of the data points derived from the S2-RF model tend to underestimate biomass. The seasonal plot of the representative paddocks (Figure 8) confirms this pattern of overestimation by the UAS and underestimation by the S2-RF model. The S2-RF model, which uses coarser resolution data, might underestimate due to the averaging effects of larger pixels or temporal mismatch (Figure 8). The overestimation and underestimation in the UAS model are attributed to the sensitivity

of 3D photogrammetry to structural vegetation changes, such as grass clumping, being laid over by wind, or the flattening of biomass due to the regenerative grazing practices used in this study.

The S2-RF model demonstrates greater accuracy when imagery acquisition is closer to the date of field sampling. For instance, Sentinel-2 imagery acquired on 24 April 2022, compared with sampled biomass on 26 April 2022 in Vault-2 (Figure 8), estimated biomass at 2339 kg DM/ha, closely matching the sampled biomass of 2506 kg DM/ha. On the same date, biomass predicted from UAS was greater (3530 kg DM/ha), illustrating the tendency of UAS to overestimate biomass, particularly when actual biomass was low (Figure 9).

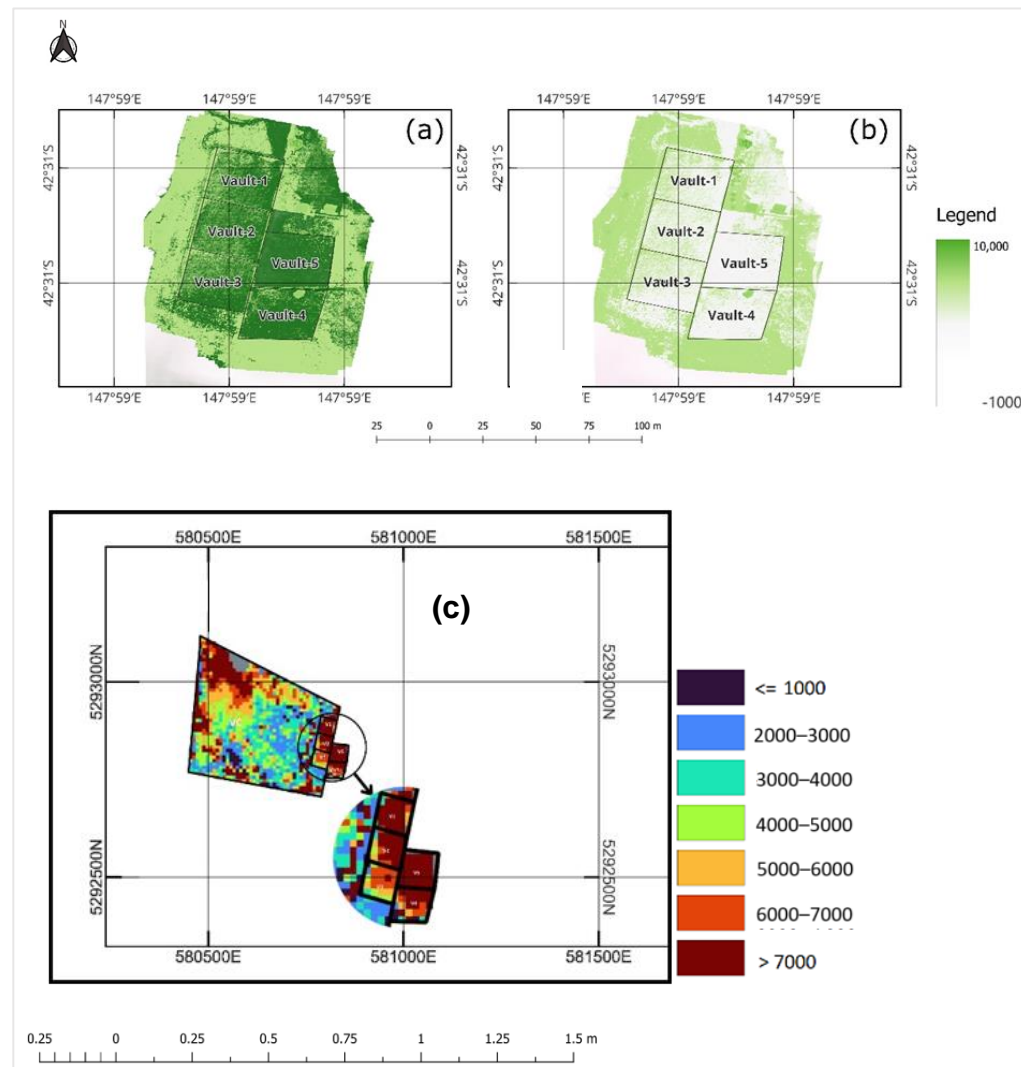


**Figure 9.** Pixel-based comparison and spatial resolution between the RGB fitted-UAS and Sentinel-2 instruments deployed for investigating grassland biomass at Okehampton in Triabunna, Australia. The field size is 0.25 ha. (a) RGB (red, green, and blue) image for pre-graze on 25 January 2023 for the Vault paddocks, (b) post-grazing event on 27 January 2023, and (c) Sentinel-2 image available on 24 January 2023. Field biomass was sampled on 25 January 2023. Units of each legend are shown in kg DM/ha. Note: The Sentinel-2 image (c) was enlarged for improved visual clarity.

Botanical composition and biomass across seasons are shown in Figure 10. Sward productivity is influenced by the collective contribution of all species, rather than by any single species. While visual assessment of species by % ranking helps to understand the variability of grassland biomass across paddocks, this ranking process is unsuitable for training satellite or drone mapping algorithms.

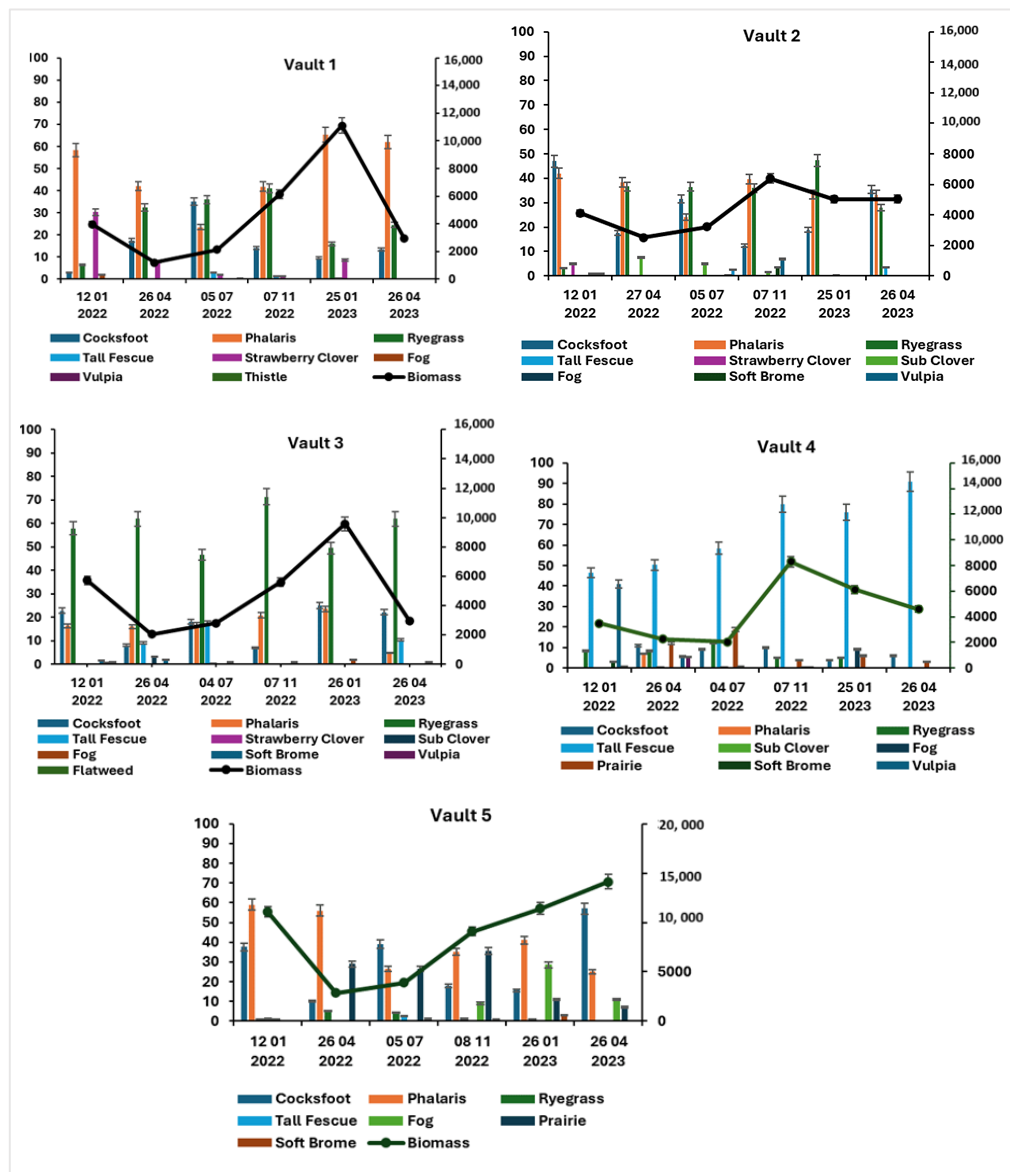


**Figure 10.** Botanical composition as a contribution toward grassland biomass in each paddock. Note: scaling is unique to each paddock as species distribution differs across plots.

### 3.2. Sentinel-2 Derived NDVI

NDVI responded positively to weekly rainfall and management interventions, such as weed control in both paddocks, with a peak rainfall observed on 21 October 2019 (Figure 11). This indicates that NDVI can effectively detect changes in vegetation cover resulting from rainfall and grazing intensity treatment. The productivity of Phalaris species in the Cottage paddock was notably higher compared to the Old Bougainville paddock, demonstrating more vigour and recovery from spring grazing (Figure 11).

Despite higher stocking density in the Cottage paddock, selective grazing on Phalaris and Cocksfoot species was not evident, likely due to the paddock being open to adjoining areas, allowing sheep to graze more freely. This results in minimal impact from high stocking density on the Cottage paddock. A decrease in NDVI and selective grazing on Cocksfoot was observed compared to Phalaris when sheep were moved to adjoining paddocks. In contrast, the Old Bougainville paddock exhibited selective grazing, particularly on Cocksfoot species, as shown by the reduction in pasture height from 5 cm to 2 cm (Figure 11). The arrival of lambs and subsequent increase in stocking rate intensified grazing intensity, leading to a decrease in NDVI values on 4 November 2019, indicating potential overgrazing in the paddock.

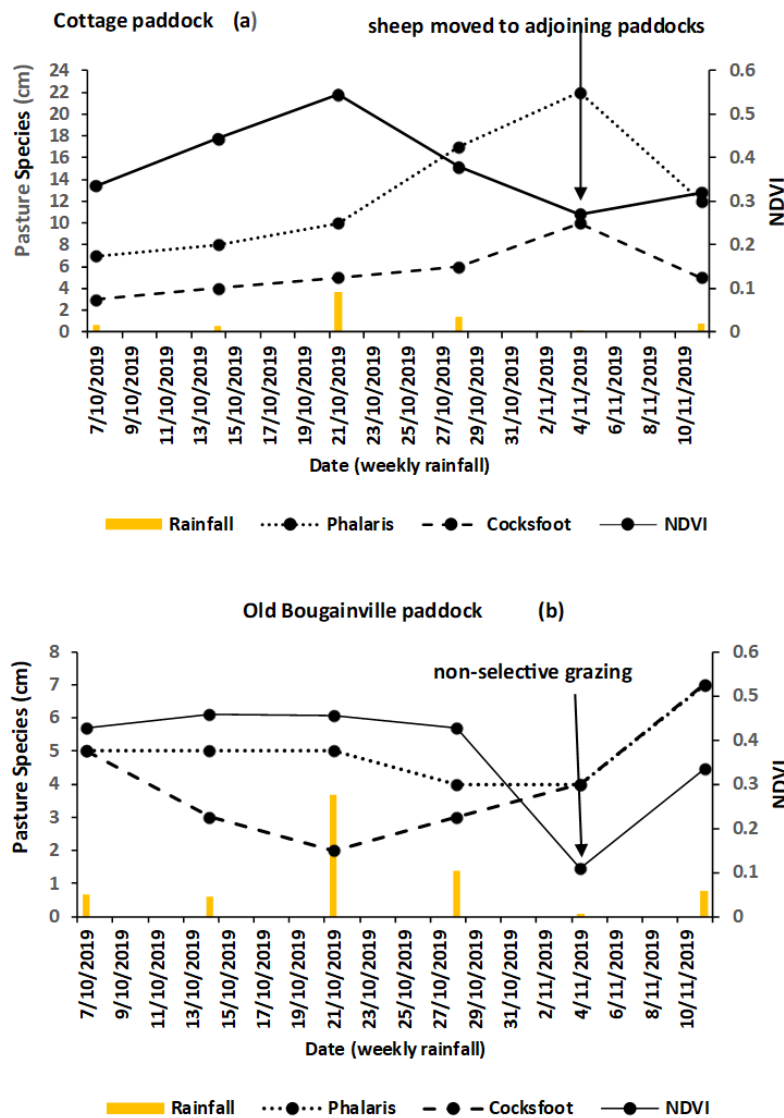


**Figure 11.** NDVI response to weekly rainfall and grazing management in Cottage and Old Bougainville paddocks, highlighting pasture species productivity and grazing patterns. The Cottage paddock (a) was used as business-as-usual by opening its gate to adjoining paddocks. Pasture species show peak heights when sheep move to adjoining paddocks. The Old Bougainville paddock (b) shows non-selective grazing from increased stocking rates (ewes that were lambing).

Weekly rainfall showed a strong correlation with NDVI changes in the Cottage paddock ( $R^2 = 0.73$ ) (Figure 12), indicating that rainfall significantly influenced pasture productivity, particularly for the Phalaris species. However, in Old Bougainville, the correlation between rainfall and NDVI was weaker ( $R^2 = 0.27$ ), primarily due to intensity grazing on the Cocksfoot species, which did not correspond to the rainfall pattern and NDVI values (Figure 12). The strong correlation between rainfall and NDVI in the Cottage paddock is likely influenced by its topography. The Cottage paddock, situated on flat terrain, experience more uniform water distribution and retention compared to the Bougainville paddock, which is located on a hilltop. The elevation position of Old Bougainville could lead to faster runoff and less water retention, thereby reducing the effectiveness of rainfall on NDVI in this paddock. The topographical difference aligns with the observed variation in the correlation between rainfall and NDVI in the two paddocks.

The interaction between rainfall and NDVI shows a strong positive correlation between rainfall and NDVI (Figure 12), while no correlation was observed between NDVI and botanical composition (Figure 13).

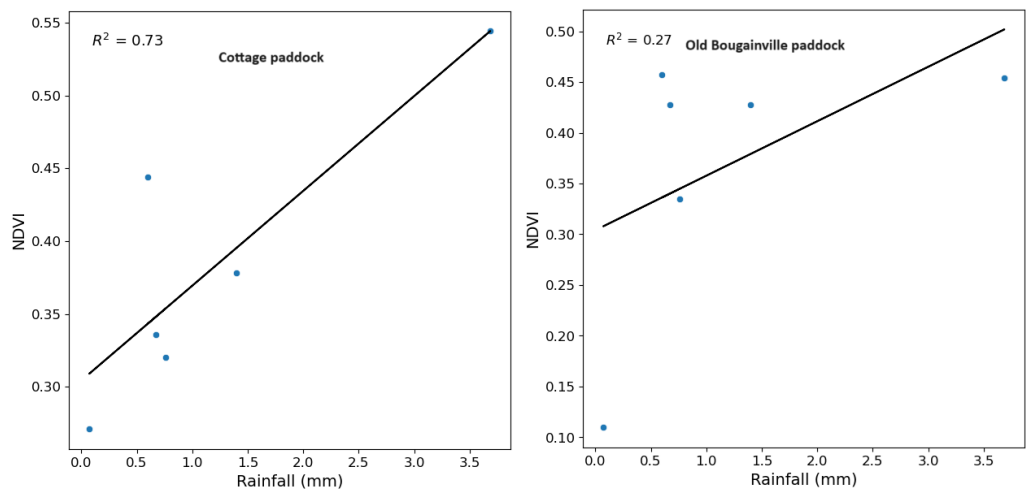


**Figure 12.** Correlation between weekly rainfall and NDVI response, highlighting the significant relationship in the Cottage and Old Bougainville paddocks during the spring of 2019 in Okehampton, Triabunna, Australia. Each data point represents the average NDVI and cumulative rainfall for that week.

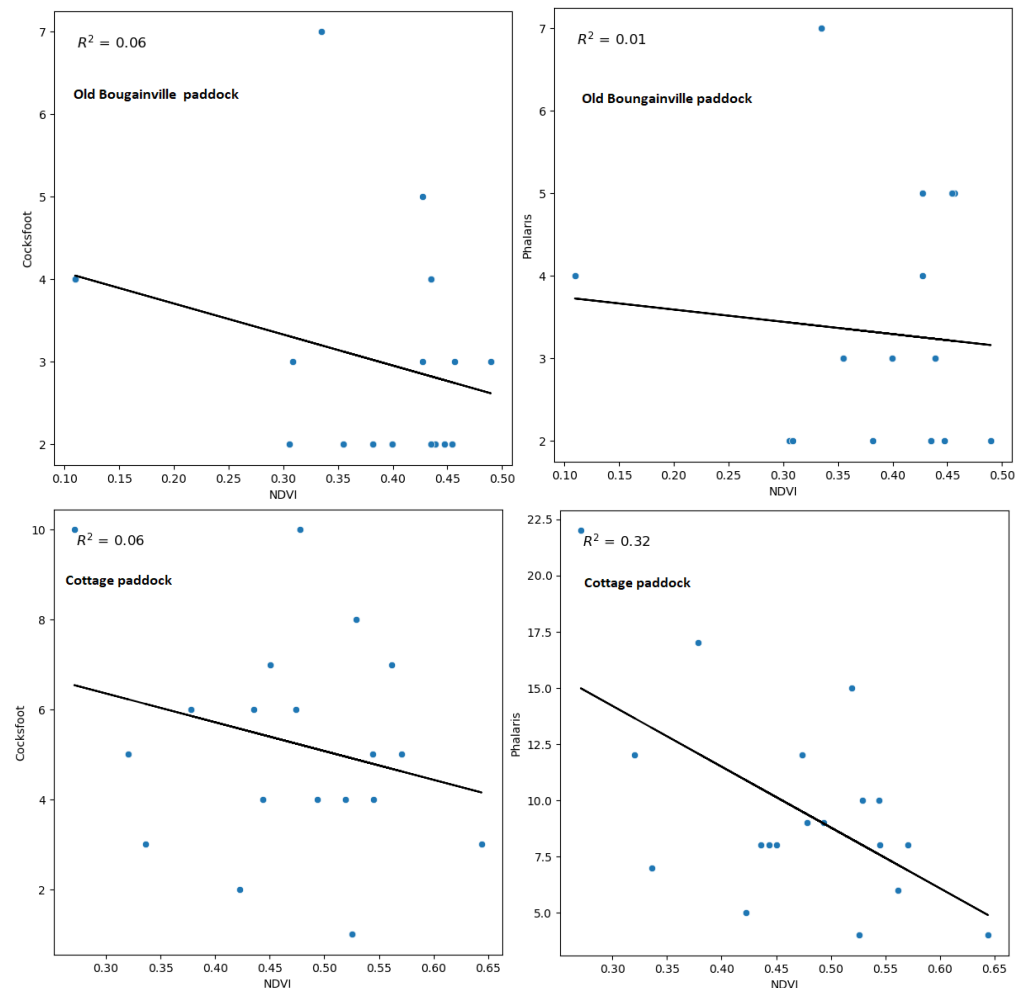


**Figure 13.** Correlation between NDVI and pasture species (Phalaris and Cocksfoot) indicates a varying relationship influenced by grazing intensity and management practices. No statistical correlation was observed between NDVI and botanical composition. The moderate correlation between Phalaris species and NDVI indicates dominance of the said species in the Cottage paddock.

## 4. Discussion

### 4.1. Grassland Biomass Modelling from a Change in Grass Heights Using 3D Photogrammetry and Sentinel-2 Imagery with the Random Forest Algorithm

Here we demonstrated the capability of remote sensing from Sentinel-2 and UAS imagery for adaptive real-time management of grasslands. If adopted, this approach would contribute to biodiversity conservation, improved grazing utilisation, and potentially improved management sustainability [5,12,17,48]. A key insight of the present study was that integration of UAS data, available on demand for pre- and post-grazing events, can enhance the performance of Sentinel-2 imagery, as illustrated in Figure 7. We applied cell grazing approaches in the field, where very high livestock stocking densities were used to flatten pasture biomass, with the aim of improving grassland productivity [12,49] and carbon and nutrient recycling [38,50], before moving sheep to the adjacent paddock in rotational grazing management. Monitoring singular, intense grazing regimes with the 5-day revisit of Sentinel-2 imagery is challenging, particularly when frequent cloud cover obscures the time between clear satellite imagery [2,51]. Even in places with fewer clouds, grassland growth responds dynamically to environmental variables (particularly rainfall and nutrient addition) [52,53], suggesting that Sentinel-2 with 5-day pass rates may be too infrequent [34]. To determine whether more timely monitoring would close this gap, we used higher-resolution UAS data to calibrate and validate Sentinel-2 models, thereby addressing the challenge of cloud contamination and enhancing biomass monitoring capabilities.

We used RMSE to assess the magnitude of errors, as it is more sensitive to larger deviations between predicted and actual biomass, while MAE provided a more straightforward measure of average error, offering a balanced view of model performance.  $R^2$  tends to emphasise the strength of the linear relationship, while RMSE provides a more practical measure of how well the model predicts actual biomass values [54]. Additionally, comparing the model's RMSE with the SEM of physical measurements helps determine whether the model performs better or worse than the expected variability in the field data [55]. The combination of these metrics allowed us to capture large and small prediction errors effectively, ensuring a more comprehensive evaluation of our models. The calibration of UAS biomass using field measurements from delta sward height through 3D photogrammetry, and the validation of Sentinel-2, produced stronger regression metrics ( $R^2 = 0.75$ , RMSE = 1240 kg DM/ha, and MAE = 980 kg DM/ha) (Figure 5) and (RMSE = 1370 kg DM/ha and MAE = 1135 kg DM/ha) compared with using the Sentinel-2 random forest-enabled model alone, ( $R^2 = 0.56$ , RMSE = 2140 kg DM/ha, and MAE = 1585 kg DM/ha). The lower  $R^2$  of 0.46 when UAS was used with Sentinel-2 compared to an  $R^2$  of 0.56 when Sentinel was used alone may be due to compounded errors (in satellite prediction of biomass, drone imagery prediction of pasture height, smaller field biomass datasets, and subsequent conversion to pasture biomass). Lower RMSE of the combined UAS-S2RF approach suggests that predictions from this approach are more accurate overall [33,54,56]. It is important to note that although the RMSE of the UAS model is slightly higher (1240 kg DM/ha) than the SEM of the field biomass (1020 kg DM/ha) (Figure 5), integrating the calibrated drone data with Sentinel-2 reduced the SEM of the S2RF model from 1642 kg DM/ha to 1473 kg DM/ha (Figures 6 and 7). Previous studies have suggested that comparing RMSE with the standard error provides a complete understanding of modelling complex ecological datasets [57].

The findings indicate that Sentinel-2, despite its moderate spatial resolution, provides robust insights into biomass variation when imagery acquisition aligns with grazing events (Figure 8). Unlike UAS, whose high resolution may be confounded by field heterogeneity, Sentinel-2 excels in capturing broader spatial and temporal patterns. Covariates such as field heterogeneity and seasonal and environmental variables may have confounded the RGB camera, despite the high resolution of the UAS instrument [2,16].

We conducted temporal analysis to examine how pasture biomass responds following grazing events, combined with statistical modelling to understand the temporal dynamics and machine learning effects in grazing management. The study by Gillan et al. [16] invoke

a similar approach (i.e., changes in sward heights) to estimate forage utilisation with UAS at a spatial resolution of 10 mm, achieving an  $R^2$  of 0.78 compared with the traditional method. Our study expanded on the utility of UAS photogrammetry models by integrating them with Sentinel-2 imagery to balance trade-offs between spectral and spatial resolutions, enabling on-demand monitoring of grazing [2].

We acknowledge the constraints imposed by the small dataset used in this study. Effective machine learning workflows often rely on robust datasets [33,58]. However, destructive biomass sampling in intensive grazing systems is frequently limited by logistical challenges [2], as was the case in this field trial. While preliminary tests with XGBoost, another model suited for small datasets, were conducted, the random forest model outperformed it in capturing the specific characteristics of our dataset. The random forest's ability to prevent overfitting and handle complex interactions made it more effective in modelling Sentinel-2 surface reflectance data and capturing biomass variability. These findings align with previous studies that have demonstrated the suitability of random forest for small datasets [59–61]. This reinforces its utility in studies constrained by limited field measurements. Future studies could build on our approach by incorporating more extensive ground datasets to enhance model performance and generalisability.

The current study faced limitations in capturing post-grazing events due to logistical challenges inherent in the traditional field sampling method. In contrast, the drone campaigns considered pre- and post-grazing data, and the Sentinel-2 method helped determine the implications of any given grazing event for biomass availability, including biomass trampled through high stocking density, and left standing, and utilised in relation to livestock productivity [2,49,62,63]. Feed utilisation in regenerative grazing provides a generic application to livestock grazing efficiency beyond the scope of 1 day as presented in this study. Ideally, feed utilisation represents feed intake by the livestock through pre- and post-grazing. Our approach considers feed utilisation by subtracting trampled (flattened) biomass after grazing from the standing biomass before grazing [12]. This process ensures liveweight gain and animal welfare through efficient feed intake, while promoting environmental stewardship by pushing unconsumed biomass down to the soil through high stocking density. This practice facilitates carbon storage, soil microbial stimulation and aggregation, and bare-ground prevention [12,38,64].

#### 4.2. Modelling Grazing Intensity and Ground Cover Productivity Using Sentinel-2-Derived NDVI

We demonstrated that NDVI effectively detects vegetation dynamics and variability due to different grazing management practices. These were applied to promote uniform or non-selective grazing, preventing the dominance of either Phalaris or Cocksfoot, while also stimulating native species. More intense grazing events during late spring or summer (October to December) to manage soil fertility decline and weed encroachment [65–67] were employed with varying stocking densities. Based on the optimal season for lambing [68,69], the stocking density was increased in the Old Bougainville paddock to intensify grazing, while the Cottage paddock was left open to the adjoining areas as a business-as-usual control. Selective grazing was observed on Phalaris species in the Old Bougainville paddock. In contrast, the low pasture cover species (Phalaris and Cocksfoot) in the Cottage, as seen in Figure 11, caused livestock to move to adjoining paddocks with more abundant pasture cover [35].

While NDVI did not correlate strongly with individual species (e.g., Phalaris and Cocksfoot) in Figures 12 and 13, this result explains the complexity of using NDVI to monitor vegetation in heterogeneous paddocks [70–72]. The variability in ground cover, including contributions from bare ground and dominant species within the GPS quadrat locations, likely reduced the sensitivity of NDVI to these specific species. This finding highlights a key challenge when using NDVI in mixed-species systems, where the index reflects the collective canopy cover rather than isolated species contributions [2]. In contrast, NDVI's higher correlation with total ground cover productivity (Figure 10) and rainfall (Figure 12) demonstrates its utility as an effective indicator of broader vegetation dynamics.

For example, the stronger relationship in the Cottage paddock ( $R^2 = 0.73$ ) compared to the Old Bougainville paddock ( $R^2 = 0.27$ ) is attributable to topographical characteristics, which influenced water distribution and retention [73]. These results emphasise the importance of considering environmental and management factors when interpreting NDVI data [73].

Despite its utility in monitoring broader vegetation dynamics, NDVI has inherent limitations when applied to mixed-species systems, particularly in grazed paddocks with heterogeneous canopy structures [2]. One key challenge is NDVI's inability to distinguish between species compositions within a canopy [70,74]. In mixed pastures, the spectral response captured by NDVI primarily reflects overall ground cover and greenness, often masking the contributions of specific species or bare ground patches. This limitation becomes more pronounced in systems where species dominance fluctuates due to grazing pressure or environmental factors. For instance, selective grazing, as observed in the Old Bougainville paddock, reduced NDVI sensitivity to individual species, highlighting the difficulty of using NDVI as a stand-alone indicator in diverse grassland systems.

Furthermore, NDVI's dependency on canopy structure and chlorophyll content means it is less effective in scenarios where plant health or cover does not directly translate to productivity [2]. For example, in areas with high soil fertility, water retention or water-logging due to topography, NDVI might overestimate vegetation health despite actual species-level declines [73,75]. These challenges underscore the need for complementary approaches, such as integrating NDVI with biophysical models or higher-resolution vegetation indices (e.g., EVI, SAVI, or NDMI), to better capture heterogeneity in mixed-species systems [76–78].

Practically, NDVI-based management requires careful calibration to account for local environmental variables, such as soil type, water availability, and grazing pressure. Site-specific adjustments, such as stratifying paddocks based on dominant species or topographical features, could enhance NDVI's applicability. Additionally, leveraging other spectral indices alongside NDVI may improve its sensitivity to species-specific responses, enabling more precise adaptive grazing management strategies. Recognising these limitations and integrating NDVI with other data sources can help overcome its current constraints, enhancing its effectiveness as a tool for sustainable pasture management in mixed-species systems.

## 5. Conclusions

This study expands the scope of grassland ecosystem monitoring by leveraging high-resolution UAS (5 mm) in high-latitude environments using 3D photogrammetry, alongside Sentinel-2 imagery. The UAS provided on-demand, pre- and post-grazing sward height, which are unattainable through Sentinel-2 imagery. Field measurement campaigns, constrained to pre-grazing data collection due to logistical challenges, were complemented by UAS data. Actual field measurements were used to calibrate the height changes captured by the 3D photogrammetry model, converting them into grassland biomass (kg DM/ha) through regression modelling. This calibration allowed for the quantification of feed intake by accounting for both pre- and post-grazing activities. It also implies that height can be effectively used as a proxy for estimating biomass.

Sentinel-2 imagery calibrated with actual field biomass using the random forest algorithm provided insights into available feed and pre-grazing grassland conditions. We showed that in high-latitude environments (such as Tasmania, Australia), Sentinel-2 imagery is often limited by frequent cloud cover, hindering temporal alignment with field measurements, rendering such imagery incapable of capturing post-grazing activities. To improve satellite estimates and validation, we used the change in biomass from the drone calibration. This multi-source remote sensing approach ensures seamless data integration, minimising temporal mismatch.

While our rationale for using 3D photogrammetry was based on high resolution for accuracy and cost-effectiveness, future studies could consider using multispectral cameras with a broader spectrum to better quantify spatial variability of field biomass.

UAS equipped with multispectral cameras can also be compared with LiDAR. Unlike 3D photogrammetry, LiDAR does not often require installation of ground control points, potentially reducing costs and labour intensity. LiDAR also provides more precise elevation data and vegetation height prognostics by penetrating canopies.

Lastly, the visual ranking of pasture species within each quadrant provided only qualitative information about pasture productivity and could not be integrated into the UAS or Sentinel-2 systems. Future studies should focus on developing methods that provide quantitative training data for more accurate mapping.

**Author Contributions:** Conceptualization, Methodology, Software, Formal Analysis, Investigation, Writing—Original Draft Preparation, Review and Visualisation, M.G.O. and M.T.H.; UAS flight campaign and processing, D.T.; Review and Editing, A.M.F.; Review and Editing, C.M.; Resources and Logistics, J.W.; Funding, M.T.H. All authors have read and agreed to the published version of the manuscript.

**Funding:** This work was funded by the Australian Government’s Future Drought Fund and the University of Tasmania (Project Number 4-G37I1PA).

**Data Availability Statement:** All data are available from the corresponding author on request.

**Acknowledgments:** The authors acknowledge project delivery and infrastructure from Cape Herbert Pty Ltd., Australia. Special acknowledgment to Peter Ball, who collected the data in the field.

**Conflicts of Interest:** Author Jason Whitehead was employed by Cape Herbert Pty Ltd. The funders had no role in the design of the study; in the collection, analyses, or interpretation of data; in the writing of the manuscript; or in the decision to publish the results.

## References

1. Luscier, J.D.; Thompson, W.L.; Wilson, J.M.; Gorham, B.E.; Dragut, L.D. Using Digital Photographs and Object-Based Image Analysis to Estimate Percent Ground Cover in Vegetation Plots. *Front. Ecol. Environ.* **2006**, *4*, 408–413. [[CrossRef](#)]
2. Ogungbuyi, M.G.; Mohammed, C.; Ara, I.; Fischer, A.M.; Harrison, M.T. Advancing Skyborne Technologies and High-Resolution Satellites for Pasture Monitoring and Improved Management: A Review. *Remote Sens.* **2023**, *15*, 4866. [[CrossRef](#)]
3. Harrison, M.T.; Cullen, B.R.; Mayberry, D.E.; Cowie, A.L.; Bilotto, F.; Badgery, W.B.; Liu, K.; Davison, T.; Christie, K.M.; Muleke, A.; et al. Carbon Myopia: The Urgent Need for Integrated Social, Economic and Environmental Action in the Livestock Sector. *Glob. Chang. Biol.* **2021**, *27*, 5726–5761. [[CrossRef](#)] [[PubMed](#)]
4. Meier, E.A.; Thorburn, P.J.; Bell, L.W.; Harrison, M.T.; Biggs, J.S. Greenhouse Gas Emissions From Cropping and Grazed Pastures Are Similar: A Simulation Analysis in Australia. *Front. Sustain. Food Syst.* **2020**, *3*, 121. [[CrossRef](#)]
5. Gillan, J.K.; Karl, J.W.; Duniway, M.; Elaksher, A. Modeling Vegetation Heights from High Resolution Stereo Aerial Photography: An Application for Broad-Scale Rangeland Monitoring. *J. Environ. Manag.* **2014**, *144*, 226–235. [[CrossRef](#)] [[PubMed](#)]
6. Cunliffe, A.M.; Brazier, R.E.; Anderson, K. Ultra-Fine Grain Landscape-Scale Quantification of Dryland Vegetation Structure with Drone-Acquired Structure-from-Motion Photogrammetry. *Remote Sens. Environ.* **2016**, *183*, 129–143. [[CrossRef](#)]
7. Harrison, M.T. Climate Change Benefits Negated by Extreme Heat. *Nat. Food* **2021**, *2*, 855–856. [[CrossRef](#)] [[PubMed](#)]
8. Fleming, A.; O’Grady, A.P.; Stitzlein, C.; Ogilvy, S.; Mendham, D.; Harrison, M.T. Improving Acceptance of Natural Capital Accounting in Land Use Decision Making: Barriers and Opportunities. *Ecol. Econ.* **2022**, *200*, 107510. [[CrossRef](#)]
9. Chang-Fung-Martel, J.; Harrison, M.T.; Brown, J.N.; Rawnsley, R.; Smith, A.P.; Meinke, H. Negative Relationship between Dry Matter Intake and the Temperature-Humidity Index with Increasing Heat Stress in Cattle: A Global Meta-Analysis. *Int. J. Biometeorol.* **2021**, *65*, 2099–2109. [[CrossRef](#)] [[PubMed](#)]
10. Wei, C.; Guo, Z.Y.; Wu, J.P.; Ye, S.F. Constructing an Assessment Indices System to Analyze Integrated Regional Carrying Capacity in the Coastal Zones—A Case in Nantong. *Ocean Coast. Manag.* **2014**, *93*, 51–59. [[CrossRef](#)]
11. Bell, L.W.; Harrison, M.T.; Kirkegaard, J.A. Dual-Purpose Cropping—Capitalising on Potential Grain Crop Grazing to Enhance Mixed-Farming Profitability. *Crop Pasture Sci.* **2015**, *66*, 2–4. [[CrossRef](#)]
12. Ogungbuyi, M.G.; Guerschman, J.P.; Fischer, A.M.; Crabbe, R.A.; Mohammed, C.; Scarth, P.; Tickle, P.; Whitehead, J.; Harrison, M.T. Enabling Regenerative Agriculture Using Remote Sensing and Machine Learning. *Land* **2023**, *12*, 1142. [[CrossRef](#)]
13. Shahpari, S.; Allison, J.; Harrison, M.T.; Stanley, R. An Integrated Economic, Environmental and Social Approach to Agricultural Land-Use Planning. *Land* **2021**, *10*, 364. [[CrossRef](#)]
14. Bai, Z.G.; Dent, D.L.; Olsson, L.; Schaepman, M.E. *Global Assessment of Land Degradation and Improvement 1. Identification by Remote Sensing*; ISRIC—World Soil Information: Wageningen, The Netherlands, 2008.
15. Zhang, C.; Kovacs, J.M. The Application of Small Unmanned Aerial Systems for Precision Agriculture: A Review. *Precis. Agric.* **2012**, *13*, 693–712. [[CrossRef](#)]
16. Gillan, J.K.; McClaran, M.P.; Swetnam, T.L.; Heilman, P. Estimating Forage Utilization with Drone-Based Photogrammetric Point Clouds. *Rangel. Ecol. Manag.* **2019**, *72*, 575–585. [[CrossRef](#)]

17. Gillan, J.K.; Karl, J.W.; van Leeuwen, W.J.D. Integrating Drone Imagery with Existing Rangeland Monitoring Programs. *Environ. Monit. Assess.* **2020**, *192*, 269. [[CrossRef](#)]
18. Liu, H.; Dahlgren, R.A.; Larsen, R.E.; Devine, S.M.; Roche, L.M.; O' Geen, A.T.; Wong, A.J.Y.; Covello, S.; Jin, Y. Estimating Rangeland Forage Production Using Remote Sensing Data from a Small Unmanned Aerial System (SUAS) and Planetscope Satellite. *Remote Sens.* **2019**, *11*, 595. [[CrossRef](#)]
19. De Rosa, D.; Bassi, B.; Fasioli, M.; Friedl, J.; Fulkerson, B.; Grace, P.R.; Rowlings, D.W. Predicting Pasture Biomass Using a Statistical Model and Machine Learning Algorithm Implemented with Remotely Sensed Imagery. *Comput. Electron. Agric.* **2021**, *180*, 105880. [[CrossRef](#)]
20. Sibanda, M.; Mutanga, O.; Rouget, M. Comparing the Spectral Settings of the New Generation Broad and Narrow Band Sensors in Estimating Biomass of Native Grasses Grown under Different Management Practices. *GIScience Remote Sens.* **2016**, *53*, 614–633. [[CrossRef](#)]
21. Wang, D.; Wan, B.; Liu, J.; Su, Y.; Guo, Q.; Qiu, P.; Wu, X. Estimating Aboveground Biomass of the Mangrove Forests on Northeast Hainan Island in China Using an Upscaling Method from Field Plots, UAV-LiDAR Data and Sentinel-2 Imagery. *Int. J. Appl. Earth Obs. Geoinf.* **2020**, *85*, 101986. [[CrossRef](#)]
22. Zlinszky, A.; Schroiff, A.; Kania, A.; Déák, B.; Mücke, W.; Vári, Á.; Székely, B.; Pfeifer, N. Categorizing Grassland Vegetation with Full-Waveform Airborne Laser Scanning: A Feasibility Study for Detecting Natura 2000 Habitat Types. *Remote Sens.* **2014**, *6*, 8056–8087. [[CrossRef](#)]
23. Madsen, B.; Treier, U.A.; Zlinszky, A.; Lucieer, A.; Normand, S. Detecting Shrub Encroachment in Seminatural Grasslands Using UAS LiDAR. *Ecol. Evol.* **2020**, *10*, 4876–4902. [[CrossRef](#)] [[PubMed](#)]
24. Jensen, J.L.R.; Mathews, A.J. Assessment of Image-Based Point Cloud Products to Generate a Bare Earth Surface and Estimate Canopy Heights in a Woodland Ecosystem. *Remote Sens.* **2016**, *8*, 50. [[CrossRef](#)]
25. Olsoy, P.J.; Shipley, L.A.; Rachlow, J.L.; Forbey, J.S.; Glenn, N.F.; Burgess, M.A.; Thornton, D.H. Unmanned Aerial Systems Measure Structural Habitat Features for Wildlife across Multiple Scales. *Methods Ecol. Evol.* **2018**, *9*, 594–604. [[CrossRef](#)]
26. Swetnam, T.L.; Gillan, J.K.; Sankey, T.T.; McClaran, M.P.; Nichols, M.H.; Heilman, P.; McVay, J. Considerations for Achieving Cross-Platform Point Cloud Data Fusion across Different Dryland Ecosystem Structural States. *Front. Plant Sci.* **2018**, *8*, 2144. [[CrossRef](#)]
27. Li, F.; Zhao, Y.; Zheng, J.; Luo, J.; Zhang, X. Monitoring Grazing Intensity: An Experiment with Canopy Spectra Applied to Satellite Remote Sensing. *J. Appl. Remote Sens.* **2016**, *10*, 026032. [[CrossRef](#)]
28. Yan, W.Y.; Shaker, A.; El-Ashmawy, N. Urban Land Cover Classification Using Airborne LiDAR Data: A Review. *Remote Sens. Environ.* **2015**, *158*, 295–310. [[CrossRef](#)]
29. Torre-Tojal, L.; Bastarrika, A.; Boyano, A.; Lopez-Gude, J.M.; Graña, M. Above-Ground Biomass Estimation from LiDAR Data Using Random Forest Algorithms. *J. Comput. Sci.* **2022**, *58*, 101517. [[CrossRef](#)]
30. Štroner, M.; Urban, R.; Křemen, T.; Braun, J. UAV DTM Acquisition in a Forested Area—Comparison of Low-Cost Photogrammetry (DJI Zenmuse P1) and LiDAR Solutions (DJI Zenmuse L1). *Eur. J. Remote Sens.* **2023**, *56*, 2179942. [[CrossRef](#)]
31. Bhattacharai, D.; Lucieer, A. Optimising Camera and Flight Settings for Ultrafine Resolution Mapping of Artificial Night-Time Lights Using an Unoccupied Aerial System. *Drone Syst. Appl.* **2024**, *12*, 1–11. [[CrossRef](#)]
32. Alvarez-Hess, P.S.; Thomson, A.L.; Karunaratne, S.B.; Douglas, M.L.; Wright, M.M.; Heard, J.W.; Jacobs, J.L.; Morse-McNabb, E.M.; Wales, W.J.; Auldist, M.J. Using Multispectral Data from an Unmanned Aerial System to Estimate Pasture Depletion during Grazing. *Anim. Feed Sci. Technol.* **2021**, *275*, 114880. [[CrossRef](#)]
33. Ogungbuyi, M.G.; Guerschman, J.; Fischer, A.M.; Crabbe, R.A.; Ara, I.; Mohammed, C.; Scarth, P.; Tickle, P.; Whitehead, J.; Harrison, M.T. Improvement of Pasture Biomass Modelling Using High-Resolution Satellite Imagery and Machine Learning. *J. Environ. Manag.* **2024**, *356*, 120564. [[CrossRef](#)] [[PubMed](#)]
34. Chen, Y.; Guerschman, J.; Shendryk, Y.; Henry, D.; Harrison, M.T. Estimating Pasture Biomass Using Sentinel-2 Imagery and Machine Learning. *Remote Sens.* **2021**, *13*, 603. [[CrossRef](#)]
35. Ara, I.; Harrison, M.T.; Whitehead, J.; Waldner, F.; Bridle, K.; Gilfedder, L.; Marques Da Silva, J.; Marques, F.; Rawnsley, R. Modelling Seasonal Pasture Growth and Botanical Composition at the Paddock Scale with Satellite Imagery. *In Silico Plants* **2021**, *3*, diaa013. [[CrossRef](#)]
36. Franklin, M. *Okehampton-Optimising Management of Production and Biodiversity Assets*; Devonport TAS; University of Tasmania: Tasmania, Australia, 2019.
37. Teague, R.; Barnes, M. Grazing Management That Regenerates Ecosystem Function and Grazingland Livelihoods. *Afr. J. Range Forage Sci.* **2017**, *34*, 77–86. [[CrossRef](#)]
38. Teague, R.; Kreuter, U. Managing Grazing to Restore Soil Health, Ecosystem Function, and Ecosystem Services. *Front. Sustain. Food Syst.* **2020**, *4*, 534187. [[CrossRef](#)]
39. Bureau of Meteorology Climate Statistics for Australian Locations. Available online: [http://www.bom.gov.au/climate/averages/tables/cw\\_092027.shtml](http://www.bom.gov.au/climate/averages/tables/cw_092027.shtml) (accessed on 25 October 2022).
40. Whalley, R.D.B.; Hardy, M.B. Measuring Botanical Composition of Grasslands. In *Field and Laboratory Methods for Grassland and Animal Production Research*; CABI Publishing: Wallingford, UK, 2000; pp. 67–102.
41. White, D.H.; Bowman, P.J. Dry Sheep Equivalents for Comparing Different Classes of Stock. *Paper* **1981**, *1530*, 81.

42. Young, J.M.; Thompson, A.N.; Curnow, M.; Oldham, C.M. Whole-Farm Profit and the Optimum Maternal Liveweight Profile of Merino Ewe Flocks Lambing in Winter and Spring Are Influenced by the Effects of Ewe Nutrition on the Progeny's Survival and Lifetime Wool Production. *Anim. Prod. Sci.* **2011**, *51*, 821–833. [[CrossRef](#)]
43. Jones, D.A.; Wang, W.; Fawcett, R. High-Quality Spatial Climate Data-Sets for Australia. *Aust. Meteorol. Oceanogr. J.* **2009**, *58*, 233–248. [[CrossRef](#)]
44. James, M.R.; Robson, S.; d’Oleire-Oltmanns, S.; Niethammer, U. Optimising UAV Topographic Surveys Processed with Structure-from-Motion: Ground Control Quality, Quantity and Bundle Adjustment. *Geomorphology* **2017**, *280*, 51–66. [[CrossRef](#)]
45. Harrison, M.T.; Whitehead, J.; Ogungbuyi, M.G.; Ball, P.; Guerschman, J.P.; Tickle, P.; Leverton, C.; Turner, D. *Operationalising Satellite and Drone Imagery to Improve Decision-Making: A Case Study with Regenerative Grazing*; University of Tasmania: Tasmania, Australia, 2023; p. 218.
46. Gillan, J.K.; Karl, J.W.; Elaksher, A.; Duniway, M.C. Fine-Resolution Repeat Topographic Surveying of Dryland Landscapes Using UAS-Based Structure-from-Motion Photogrammetry: Assessing Accuracy and Precision against Traditional Ground-Based Erosion Measurements. *Remote Sens.* **2017**, *9*, 437. [[CrossRef](#)]
47. Foga, S.C.; Scaramuzza, P.; Guo, S.; Zhu, Z.; Dilley, R.; Beckmann, T.; Schmidt, G.L.; Dwyer, J.L.; Hughes, M.J.; Laue, B. Cloud Detection Algorithm Comparison and Validation for Operational Landsat Data Products. *Remote Sens. Environ.* **2017**, *194*, 379–390. [[CrossRef](#)]
48. Langworthy, A.D.; Rawnsley, R.P.; Freeman, M.J.; Pembleton, K.G.; Corkrey, R.; Harrison, M.T.; Lane, P.A.; Henry, D.A. Potential of Summer-Active Temperate ( $C_3$ ) Perennial Forages to Mitigate the Detrimental Effects of Supraoptimal Temperatures on Summer Home-Grown Feed Production in South-Eastern Australian Dairying Regions. *Crop Pasture Sci.* **2018**, *69*, 808–820. [[CrossRef](#)]
49. Harrison, M.T.; Christie, K.M.; Rawnsley, R.P.; Eckard, R.J. Modelling Pasture Management and Livestock Genotype Interventions to Improve Whole-Farm Productivity and Reduce Greenhouse Gas Emissions Intensities. *Anim. Prod. Sci.* **2014**, *54*, 2018–2028. [[CrossRef](#)]
50. Díaz de Otálora, X.; Epelde, L.; Arranz, J.; Garbisu, C.; Ruiz, R.; Mandaluniz, N. Regenerative Rotational Grazing Management of Dairy Sheep Increases Springtime Grass Production and Topsoil Carbon Storage. *Ecol. Indic.* **2021**, *125*, 107484. [[CrossRef](#)]
51. Punalekar, S.M.; Verhoef, A.; Quaife, T.L.; Humphries, D.; Bermingham, L.; Reynolds, C.K. Application of Sentinel-2A Data for Pasture Biomass Monitoring Using a Physically Based Radiative Transfer Model. *Remote Sens. Environ.* **2018**, *218*, 207–220. [[CrossRef](#)]
52. Phelan, D.C.; Harrison, M.T.; Kemmerer, E.P.; Parsons, D. Management Opportunities for Boosting Productivity of Cool-Temperate Dairy Farms under Climate Change. *Agric. Syst.* **2015**, *138*, 46–54. [[CrossRef](#)]
53. Rawnsley, R.P.; Smith, A.P.; Christie, K.M.; Harrison, M.T.; Eckard, R.J. Current and Future Direction of Nitrogen Fertiliser Use in Australian Grazing Systems. *Crop Pasture Sci.* **2019**, *70*, 1034–1043. [[CrossRef](#)]
54. ter Braak, C.J.F.; Juggins, S. Weighted Averaging Partial Least Squares Regression (WA-PLS): An Improved Method for Reconstructing Environmental Variables from Species Assemblages. In Proceedings of the Twelfth International Diatom Symposium, Renesse, The Netherlands, 30 August–5 September 1992; Springer: Berlin/Heidelberg, Germany, 1993; pp. 485–502.
55. Bishop, T.F.A.; McBratney, A.B. A Comparison of Prediction Methods for the Creation of Field-Extent Soil Property Maps. *Geoderma* **2001**, *103*, 149–160. [[CrossRef](#)]
56. Piñeiro, G.; Perelman, S.; Guerschman, J.P.; Paruelo, J.M. How to Evaluate Models: Observed vs. Predicted or Predicted vs. Observed? *Ecol. Model.* **2008**, *216*, 316–322. [[CrossRef](#)]
57. Chai, T.; Draxler, R.R. Root Mean Square Error (RMSE) or Mean Absolute Error (MAE)?—Arguments against Avoiding RMSE in the Literature. *Geosci. Model Dev.* **2014**, *7*, 1247–1250. [[CrossRef](#)]
58. Morais, T.G.; Teixeira, R.F.M.; Figueiredo, M.; Domingos, T. The Use of Machine Learning Methods to Estimate Aboveground Biomass of Grasslands: A Review. *Ecol. Indic.* **2021**, *130*, 108081. [[CrossRef](#)]
59. Belgiu, M.; Drăguț, L. Random Forest in Remote Sensing: A Review of Applications and Future Directions. *ISPRS J. Photogramm. Remote Sens.* **2016**, *114*, 24–31. [[CrossRef](#)]
60. Mutanga, O.; Skidmore, A.K. Narrow Band Vegetation Indices Overcome the Saturation Problem in Biomass Estimation. *Int. J. Remote Sens.* **2004**, *25*, 3999–4014. [[CrossRef](#)]
61. Rodriguez-Galiano, V.F.; Ghimire, B.; Rogan, J.; Chica-Olmo, M.; Rigol-Sánchez, J.P. An Assessment of the Effectiveness of a Random Forest Classifier for Land-Cover Classification. *ISPRS J. Photogramm. Remote Sens.* **2012**, *67*, 93–104. [[CrossRef](#)]
62. Ibrahim, A.; Harrison, M.T.; Meinke, H.; Zhou, M. Examining the Yield Potential of Barley Near-Isogenic Lines Using a Genotype by Environment by Management Analysis. *Eur. J. Agron.* **2019**, *105*, 41–51. [[CrossRef](#)]
63. Taylor, C.A.; Harrison, M.T.; Telfer, M.; Eckard, R. Modelled Greenhouse Gas Emissions from Beef Cattle Grazing Irrigated Leucaena in Northern Australia. *Anim. Prod. Sci.* **2016**, *56*, 594–604. [[CrossRef](#)]
64. Henry, B.; Dalal, R.; Harrison, M.T.; Keating, B. *Creating Frameworks to Foster Soil Carbon Sequestration*; Burleigh Dodds Science Publishing: Cambridge, UK, 2022.
65. Dorrough, J.; Ash, J.; McIntyre, S. Plant Responses to Livestock Grazing Frequency in an Australian Temperate Grassland. *Ecography* **2004**, *27*, 798–810. [[CrossRef](#)]
66. Akhmadov, K.M.; Breckle, S.W.; Breckle, U. Effects of Grazing on Biodiversity, Productivity, and Soil Erosion of Alpine Pastures in Tajik Mountains. In *Land Use Change and Mountain Biodiversity*; CRC Press: Boca Raton, FL, USA, 2006; pp. 239–248.

67. Blackburn, W.H. Impacts of Grazing Intensity and Specialized Grazing Systems on Watershed Characteristics and Responses. In *Developing Strategies for Rangeland Management*; CRC Press: Boca Raton, FL, USA, 2021; pp. 927–984.
68. Allworth, M.B.; Wrigley, H.A.; Cowling, A. Fetal and Lamb Losses from Pregnancy Scanning to Lamb Marking in Commercial Sheep Flocks in Southern New South Wales. *Anim. Prod. Sci.* **2016**, *57*, 2060–2065. [[CrossRef](#)]
69. Hopkins, D.L.; Gilbert, K.D.; Saunders, K.L. The Performance of Short Scrotum and Wether Lambs Born in Winter or Spring and Run at Pasture in Northern Tasmania. *Aust. J. Exp. Agric.* **1990**, *30*, 165–170. [[CrossRef](#)]
70. Hill, M.J.; Donald, G.E.; Hyder, M.W.; Smith, R.C.G. Estimation of Pasture Growth Rate in the South West of Western Australia from AVHRR NDVI and Climate Data. *Remote Sens. Environ.* **2004**, *93*, 528–545. [[CrossRef](#)]
71. Weber, D.; Schaepman-Strub, G.; Ecker, K. Predicting Habitat Quality of Protected Dry Grasslands Using Landsat NDVI Phenology. *Ecol. Indic.* **2018**, *91*, 447–460. [[CrossRef](#)]
72. Ara, I.; Turner, L.; Harrison, M.T.; Monjardino, M.; DeVoil, P.; Rodriguez, D. Application, Adoption and Opportunities for Improving Decision Support Systems in Irrigated Agriculture: A Review. *Agric. Water Manag.* **2021**, *257*, 107161. [[CrossRef](#)]
73. Kumhálová, J.; Kumhála, F.; Kroutilík, M.; Matějková, Š. The Impact of Topography on Soil Properties and Yield and the Effects of Weather Conditions. *Precis. Agric.* **2011**, *12*, 813–830. [[CrossRef](#)]
74. An, S.; Chen, X.; Zhang, X.; Lang, W.; Ren, S.; Xu, L. Precipitation and Minimum Temperature Are Primary Climatic Controls of Alpine Grassland Autumn Phenology on the Qinghai-Tibet Plateau. *Remote Sens.* **2020**, *12*, 431. [[CrossRef](#)]
75. Liu, K.; Harrison, M.T.; Ibrahim, A.; Manik, S.M.N.; Johnson, P.; Tian, X.; Meinke, H.; Zhou, M. Genetic Factors Increasing Barley Grain Yields Under Soil Waterlogging. *Food Energy Secur.* **2020**, *9*, e238. [[CrossRef](#)]
76. Ho, C.K.M.; Jackson, T.; Harrison, M.T.; Eckard, R.J. Increasing Ewe Genetic Fecundity Improves Whole-Farm Production and Reduces Greenhouse Gas Emissions Intensities: 2. Economic Performance. *Anim. Prod. Sci.* **2014**, *54*, 1248–1253. [[CrossRef](#)]
77. Phelan, D.C.; Harrison, M.T.; McLean, G.; Cox, H.; Pembleton, K.G.; Dean, G.J.; Parsons, D.; do Amaral Richter, M.E.; Pengilley, G.; Hinton, S.J.; et al. Advancing a Farmer Decision Support Tool for Agronomic Decisions on Rainfed and Irrigated Wheat Cropping in Tasmania. *Agric. Syst.* **2018**, *167*, 113–124. [[CrossRef](#)]
78. Bilotto, F.; Harrison, M.T.; Migliorati, M.D.A.; Christie, K.M.; Rowlings, D.W.; Grace, P.R.; Smith, A.P.; Rawnsley, R.P.; Thorburn, P.J.; Eckard, R.J. Can Seasonal Soil N Mineralisation Trends Be Leveraged to Enhance Pasture Growth? *Sci. Total Environ.* **2021**, *772*, 145031. [[CrossRef](#)]

**Disclaimer/Publisher’s Note:** The statements, opinions and data contained in all publications are solely those of the individual author(s) and contributor(s) and not of MDPI and/or the editor(s). MDPI and/or the editor(s) disclaim responsibility for any injury to people or property resulting from any ideas, methods, instructions or products referred to in the content.